ATLANTIS
PRESS

Microstructure simulation and Multi-physical field Analysis of 400mm thick Continuous Casting Slabs

Pinghu Chen[1,2,a], Yibo Li[1,2,b], Xiaoqian Li[1,2,c]

[1] College of Mechanical and Electrical Engineering, Central South University, 410083, Changsha P. R. China

[2] State Key Laboratory of High Performance Complex Manufacturing, Changsha, 410083, P.R. China

[3] Light Alloy Research Institute, Central South University, 410083, Changsha P. R. China

[a] chenpinghu1986@163.com,[b] yibo.li@csu.edu.cn,[c] meel@csu.edu.cn

Keywords: Continuous casting; Casting speed; Superheat; Secondary cooling; Microstructure；Numerical simulation

Abstract: Based on the parameters were provided by a caster enterprise, Pro-cast was adopted to simulate temperature field and solidus rate of continuous casting steel about the 2400 mm×400 mm cross section. On the premise of validation of simulation method, the effects of different casting speeds, degree of superheat and secondary cooling to the microstructure have been studied by the numerical simulation. The results show that, Grain number, average grain size and maximum grain size are little changed along with the change of casting speed and secondary cooling, but average grain size decrease with the increase of superheat. The equiaxed grain ratio is unchanged with casting speed increase, is about 13.9%. The center of narrow face shell at the mold exit is thinnest and the thickness is about 10.4 mm, and increases along the wide face direction gradually. the wide face shell thickness near the corner is 18.9 mm, and the center thickness is 27.6 mm. The trend of stress change at the slab solidification front is almost consistent with temperature, demonstrating the initial solidified shell stress is mainly thermal stress. Therefore. the 20℃ superheat, 0.54m/min casting speed and low water flow rate are reasonable parameters for 400mm×2400mm extra-thick special slabs in the continuous casting. Theoretical basis is provided for the practical production in the future.

INTRODUCTION

Technology characteristic, such as low drawing speed, slow solidification and long cavity, easily lead to the continuous casting defects as segregation, looseness, cracks, low temperature of edge and corner, etc. The optimization of casting speed, superheat and cooling conditions on secondary cooling zone has an important role in improving the casting defects[1-5]. It is not sensible to establish reasonable process parameters under the circumstance of unintelligent casting equipment and immature technology maturity of continuous casting. Actual experimental trials to determine optimum conditions of operation in the continuous casting unit can lead to interruptions in the production schedule and consequently loss of productivity and profitability. Mathematical analysis and physical modeling experiments in the laboratory are an alternative to achieve optimum conditions for achieving increased productivity and improved quality of the product[5]. This method not only need long cycle, large cost and but is not conducive to the enterprise's long-term development[6].

There are many difficulties exists in manufacturing process of the extra-thick special plate, optimizing process parameters have an effective influence on the microstructure and properties. Some researchers have done a whole lot of research on temperature and flow field of wide and thick slab continuous casting, besides large round billet and square billet, and studied microstructure of round and square billets. Degree of superheat and casting speed has been considered as the two process parameters which are varied to see their effect on the solidification behavior of the cast

product[7]. R. Vertnik [8] studied turbulent fluid and solidification by the commercial software ANSYS Fluent. Zhang Jian[9] explored the effects of transverse nozzle arrangement, inter-zone distance, M. RYWOTYCKI[10] number of segments number, and length of cooling zone on temperature and stress fields of round billets. Illustrated the effects of two ways of boundary conditions (average heat transfer coefficient and complex models in primary and secondary cooling zones) on temperature change. However, microstructure evolution, nor the grain size varies on such studies, especially for the extra-thick slabs, which means above 400mm thick, have little investigated[11-13].

In this paper, effects of different casting speed, superheat and secondary cooling on the microstructure of extra-thick special plate are studied in the process of continuous casting. Finite element method combined with traveling boundary algorithm is adopted to simulate the microstructure evolution of the casting billets under CAFÉ modules of pro-cast software. multi-physical field, which means coupled fields of the mold with temperature turbulent flow are studied to verify the model and provide a theoretical foundation for optimizing the second cooling intensity of species-steel plate in the continuous casting.

1. Mathematical and physical model

1.1 Boundary conditions and assumptions

Following assumptions about the solidification model are made to simplify the governing equations:

➢ Liquid steel as Newtonian incompressible fluid.
➢ shell contact mold perfectly and contact heat transfer coefficient is very large
➢ No slip boundary condition prevails at the walls.
➢ shrinkage due to solidification is ignored.
➢ Only two dimensional heat transfers (lateral direction) is considered.
➢ Mold oscillation, bending of strand, effect of segregation, etc. have been ignored.

Material for this study is H13, all the material properties and standard conditions used for analysis are listed in **Table 1**.

Table 1 material properties and boundary conditions

Material property	*value*	*Boundary conditions, Machine parameters*	*value*
Steel density, kg.m^{-3}		*Casting speed, m/min*	0.48,0.54,0.60,0.66
Viscosity of liquid steel, kg.m^{-1}.s^{-1}		*Mould length, m*	0.9
Thermal conductivity,W.m^{-1}.K^{-1}	Variation value with temperature	*Cross-sectional dimensions, m^2*	0.4×2.4
Specific heat,J.kg.K^{-1}		*Vertical length, m*	3.106
Latent heat, J.kg^{-1}		*Horizontal length, m*	22.276
Liquidus temperature, K	1748	*Machine radius, m*	11
Solidus temperature, K	1633	*Liquid steel superheat, K*	10,20,30,40
Mushy zone constant	100000	*Water ratio, L/Kg*	0.8, 1.0, 1.2, 1.4

Fig.1 shows all the parameters for the curved casting machine in the paper. To avoid the computational difficulties, the physical model is simplified, according to symmetry of physical model, 1/2 physical model is considered for simulating the microstructure of the entire casting; 1/4 physical model is considered for simulating the multi-physical field, including the temperature field, flow field and stress field. Final model of the casting billet for this analysis is shown as **Fig.1**. The inlet velocity is only applied to meniscus in Y-direction (vertical direction). However, inlet temperature (T_{inlet}) of the molten steel was fixed according to the superheat ($\triangle T$) provided to the steel above the liquidus temperature(T_L). T_{inlet} equals $T_L+\triangle T$. the heat extraction from steel through cooling water flowing within mold, and heat transfer coefficient in secondary cooling zone was set with using traveling boundary method.
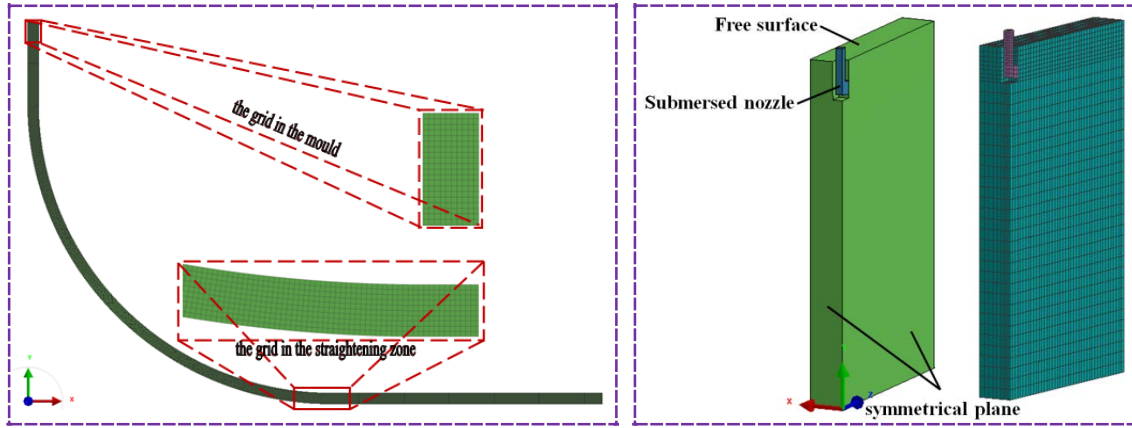
Fig.1 Geometry model and mesh model (a) overall continuous casting and (b) in the mould

1.2 Governing equations

1.2.1 Governing equation of Temperature field and flow field

Solidus temperature of the special steel is very high, and large distance from the solidification end to the meniscus. Therefore, influence of the fluid flow to the temperature change is ignored in the solidification end.effect of the temperature change on microstructure is considered in the model. Mass conservation equation for solidification can be defined as the equation (1), Momentum conservation equation(x direction, the similar as y and z direction) can be defined as the equation (2), Turbulent kinetic energy equation and Turbulent kinetic energy dissipation equation can be defined as the equation (3), Where, turbulent viscosity expression and pressure express formula can be defined as the equation (4), Energy conservation equation can be defined as the equation (5).

$$\frac{\partial \rho}{\partial t} + \frac{\partial \rho_u}{\partial x} + \frac{\partial \rho_v}{\partial y} + \frac{\partial \rho_w}{\partial z} = 0 \tag{1}$$

$$\frac{\rho}{f_l}\frac{\partial u}{\partial t} + \frac{\rho}{f_l^2}\left(u\frac{\partial u}{\partial x} + v\frac{\partial u}{\partial y} + w\frac{\partial u}{\partial z}\right) = -\frac{\partial P}{\partial x} + \rho g_x + \frac{\partial}{\partial x}\left(\frac{u}{f_l}\frac{\partial u}{\partial x}\right) + \frac{\partial}{\partial y}\left(\frac{u}{f_l}\frac{\partial u}{\partial y}\right) + \frac{\partial}{\partial z}\left(\frac{u}{f_l}\frac{\partial u}{\partial z}\right) - \left(\frac{\mu}{K}\right)u \tag{2}$$

$$\frac{\partial}{\partial t}(\rho k) + \frac{\partial}{\partial x_j}(\rho u_j k) = \rho P - \rho\varepsilon + \frac{\partial}{\partial x_j}\left[\left(\mu + \frac{\mu_T}{\sigma_k}\right)\frac{\partial k}{\partial x_j}\right]$$

$$\frac{\partial}{\partial t}(\rho\varepsilon) + \frac{\partial}{\partial x_j}(\rho u_j \varepsilon) = C_1\frac{\varepsilon}{k}\rho P - C_2\frac{\varepsilon}{k}\rho\varepsilon + \frac{\partial}{\partial x_j}\left[\left(\mu + \frac{\mu_T}{\sigma_\tau}\right)\frac{\partial\varepsilon}{\partial x_j}\right] \tag{3}$$

$$\mu_T = C_\mu\frac{k^2}{\varepsilon}, P = \mu_T\left(\frac{\partial u_i}{\partial x_j} + \frac{\partial u_j}{\partial x_i} - \frac{2}{3}\frac{\partial u_m}{\partial x_m}\delta_{ij}\right) - \frac{2}{3}k\frac{\partial u_m}{\partial x_m} \tag{4}$$

$$\rho\frac{\partial H}{\partial t} + \rho\frac{\partial H}{\partial T}\left(u\frac{\partial T}{\partial x} + v\frac{\partial T}{\partial y} + w\frac{\partial T}{\partial z}\right) = \frac{\partial}{\partial x}\left(\kappa\frac{\partial T}{\partial x}\right) + \frac{\partial}{\partial y}\left(\kappa\frac{\partial T}{\partial y}\right) + \frac{\partial}{\partial z}\left(\kappa\frac{\partial T}{\partial z}\right) \tag{5}$$

Where, u、 v and w are Velocity component of the x、 y and z direction, m·s^{-1}, respectively; f_l , f_s are Liquid fraction and Solid fraction, respectively; ρ is Density，kg·m^{-3}; P is Pressure，Pa; g_x is Gravity component of the x direction, m·s^{-2}; μ is absolute viscosity, Pa·s; K is fluid permeability, m^2; c_p is specific heat capacity, J·kg^{-1}·K^{-1}; κ is thermal conductivity, W·m^{-1}·K^{-1}; t is time, s; L is solidification latent heat, J·kg^{-1}; T is node's temperature, K; H is enthalpy, J·mol^{-1}.

1.2.2 Governing equation of Nucleation and growth model

Most of Alloy solidification are based on heterogeneous nucleation, and final grain size and shape is affected by many conditions in the solidification process. therefore, continuous distribution function dn/d(ΔT) is adopted to describe the change of the grain density. The grain density increasing dn is caused by the increase of superheat ΔT. dn/d(ΔT) be determined by the gaussian distribution[13-15], Nucleation model can be defined as the equation (6). To overwhelming majority of the alloy, there is no necessarily to consider supercooling of thermodynamics, curvature undercooling of solid-liquid interface and supercooling of growth dynamics ,and then the fitting KGT model is used for the growth rate of columnar grains and the equiaxed grains.   such a model can be defined as the equation (7).

$$N = \frac{d\Delta T}{\Delta t}\frac{n_{max}}{\sqrt{2\pi}\Delta T_\sigma}\exp\left(\frac{1}{2}\left(\frac{\Delta T - \Delta T_{max}}{\Delta T_\sigma}\right)^2\right) \tag{6}$$

$$v(\Delta T) = \alpha \Delta T^2 + \beta \Delta T^3 \qquad (7)$$

Where, ΔT_{max} is supercooling of average nucleation, ΔT_σ is standard deviation of nucleation supercooling, n_{max} is the maximum nucleation density, α and β are polynomial fitting coefficients, respectively. α is 1.49×10^{-6}, β is 2.899×10^{-6}, ΔT is degree of supercooling.

1.3 Heat transfer model

Based on ASTM criteria, $N_V = 0.8\, N_A^{3/2} = 0.569\, N_L^3$ (N_V= the grain number per unit volume, N_A= the grain number per unit area, N_L= the grain number per unit linear)[15]. In this paper, Surface nucleation density $n_{a,max} = 1 \times 10^{-7}$ m^{-2}, volume nucleation density $n_{v,max} = 2.53 \times 10^{-10}$ m^{-3}. In the mould, heat fluxes function can be defined as the equation (8). In the Secondary cooling zone, the shell is cooled directly by the cooling water, most of the empirical formula to calculate. In this paper, the secondary cooling is divided into twelve segments, each segment width surface heat transfer coefficient using. M.I shiguro[16] suggested experience equation is adopted to calculate the coefficient of heat transfer, heat transfer equation can be defined as the equation (9).

$$q = A - B\sqrt{d_y / v} \qquad (8)$$

$$h = 0.58 W^{0.451}(1 - 0.0075 T_w) \qquad (9)$$

Where, qis the heat flux, d_y is distance from any place to the meniscus in the mould, v=casting speed, A and B = the empirical constant, A = 2.509, B = 0.268 for slab width face, A = 1.559，B = 0.190 for slab narrow face, h is coefficient of heat transfer, W is water flow intensity, T_W is temperature of cooling water.

2. Simulation results and discussion

2.1 Effect of casting speed

In the first part of investigation, effect of casting speed on the microstructure morphologies has been studied. **Fig.2** shows the microstructure morphologies of cross section under the region of complete solidification at the same superheat and secondary cooling condition, the distance increases between solidifying forefront to the meniscus as casting speed rise. the end of the solidification cooling condition is relatively lower at the same location. Therefore, temperature gradient of the solid-liquid mixed area is reduced from pouring temperature to the solidification front; growth ratio of the dendrite tip is decreasing and super-cooling range is widening accordingly. the crystal nucleation may be promoted in the process, and then raising solid ratio to prevent the growth of the columnar crystal. **Fig.2** describe the microstructure properties under different casting speed(0.48m/min, 0.54m/min, 0.60m/min, 0.66m/min). Changes of equiaxed grains ratio is mild along with little velocity fluctuation. Influence of nucleation and growth is little although shell thickness decreasing at the exit of mould and Liquid core length increasing because of casting speed increasing. The result indicates Number of the grains, average grain size, maximum grain size and Average grain radius are not changing with casting speed changing. To sum up, the shell thickness should be 23.7 mm in order to prevent damage of the shell and break out accidents happening as large static pressure of liquid steel at the exit of mould. Hence, while satisfy the precondition of safety, for improving production efficiency, larger casting speed is selected. Therefore, casting speed 0.54 m/min is regard as a more appropriate casting speed.

2.2 Effect of superheat

Fig.3 demonstrates the microstructures with different degree of superheat in the same casting speed and cooling conditions. grain number, grain surface area, maximum surface area and average grain radius of the simulated microstructure results are counted. As superheat of liquid steel increases, the grain number decrease at the same location area, meanwhile average grain radius, average grain surface area and maximum surface area increased, as well as **Fig.3**, the area of columnar structure enlarged, and that of equiaxed crystals decreased. According to the statistical data, the ratio of equiaxed gain zone respectively are 16.1%, 14.93%, 13.71% and 13.34% at the superheat temperature of 10°C, 20°C, 30°Cand 40°C. A sharp drop of temperature can be seen in the mould region as heat loss from the mold is very high. Therefore, equiaxed crystals are formed at the

near face and the central region, it can also be seen that the change in superheat has a very large on number of the grains, average grain area, maximum grain area and average grain radius. With the increase of Super-cooling degree, growth of the columnar crystal is accelerated from surface to central in the cross section, development of the secondary dendrite is more efficient. The columnar grain zone expanded significantly, and the equiaxed crystal zone correspondingly narrows.
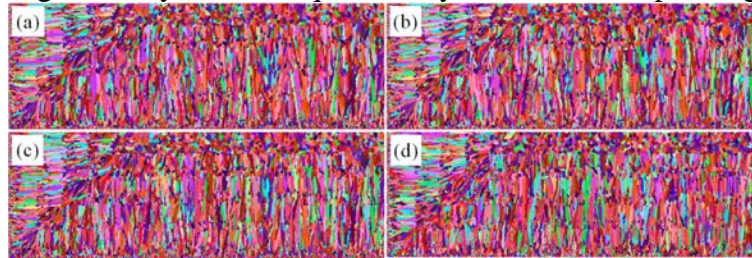
Fig.2 The results of microstructure under different casting speed.(a)0.48, (b)0.54, (c)0.60, (d)0.66 m/min
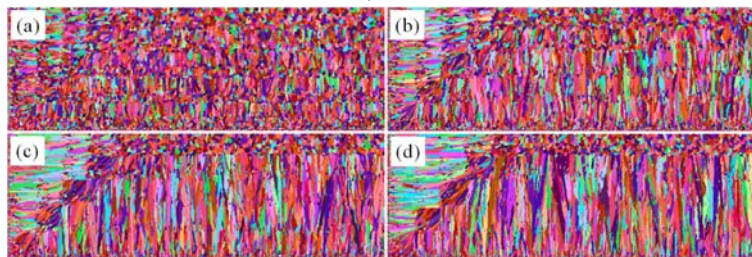
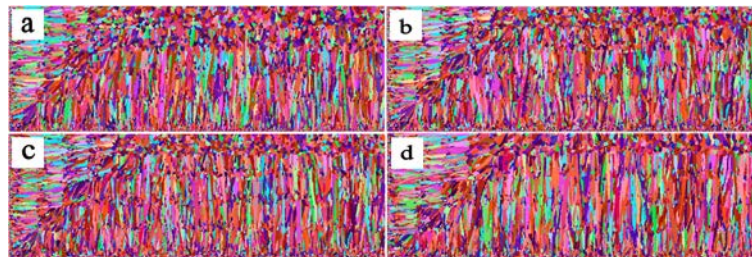Fig.3 The results of microstructure under different degree of superheat. (a) 10 °C; (b) 20 °C; (c) 30 °C; (d)40 °C

Fig.4 The results of microstructure under different specific water flow

2.3 Effect of secondary cooling

About 80% of the heat is extracted in the secondary cooling process, at which point the liquid steel is completely solidified[17]. Therefore, the equiaxed crystal number and size are determined in the secondary cooling zone. In the premise condition of the same casting speed 0.54 m/min and superheat 20°C, simulation results of solidification structure under the different secondary cooling condition, as show in **Fig.4**. Firstly, the equiaxed crystal of the chilled layer is formed in the mould, so the fine equiaxed crystal is not affected by the supercooling degree on the near face of casting slab. Secondly, along with solidifying time's increase, the heat transfer gradually decreases, which led to thick columnar crystals form. Thirdly, with the increase of special water flow, the supercooling degree increase at the solidifying forefront of the solid-liquid interface, the increase of supercooling degree is conducive to the growth of the columnar crystal, at the same time, the formation of the equiaxed crystal is inhibited in the central region of the casting ingot. but because Therefore, the equiaxed crystal of near face is no affected by special water flow of secondary cooling region. Therefore, secondary cooling water take appropriate to be reduced to inhibit the growth of the columnar crystal and to promote the growth of the equiaxed crystal in the actual process of continuous casting, thereby gaining a reasonable rate of the equiaxed crystal.

2.4 Model validation

It is necessary to correct boundary conditions for enhancing the accuracy of numerical simulation. The temperature field and solid fraction are shown in **Fig.5a**. under the conditions of casting speed 0.54m/min and superheat 20°C. The shell thickness is 23.7mm at the exit of mould and Liquid core length is 28.8m from the meniscuses to the solidification end. According to value of

the theoretical calculation, the shell thickness is 25mm and Liquid core length is 29.63m. but beyond that, through the measured data, the shell thickness is 22-26mm and the liquid core length is 26.6-30m. The results show there is a good agreement with modeled and experimental value, as shown in **Table 2**.

Table 2 the results of shell thickness and liquid core length

	Value with casting speed 0.54m/min and superheat 20℃	
	Shell thickness，mm	Liquid core length，m
Theoretical calculation	25	29.63
Experiment result	22-26	26.6-30
Simulated result	23.7	28.8

Model calculation of the microstructure is performed with Nucleation and growth model. The microstructure were calculated at 1/2 symmetrical body. Schematic diagram of evolution solidification microstructure is shown as **Fig.5b**. **Fig.5b-a** is the microstructure of longitudinal section for various distance from the meniscus, and Fig.3b is the microstructure of cross section that corresponds to **Fig.5b-a**. For the same continuous caster, cooling methods are different at the different region of continuous casting billet, such as the mould , the secondary cooling zone and air cooling zone. Accordingly, the cooling intension is not the same and presents weakening trend from the meniscus to the end. Solidification starting firstly with the dendrite growth, solute is evacuated from the dendrite arm to the under-cooling melts along with the dendrites' growth, and then is enriched around the dendrite arm. Based on the effect of surface tension of the dendrite arm and solute diffusion, solid-liquid interface of the primary dendrites arm lost its balance, thus forming secondary dendrite arm in the process of dendrite growth. By that analogy, with the solidification process and dendrite growth, higher order dendrite arms are gradually formed, Now that being said, undercooling degree of average nucleation is becoming smaller and smaller in the liquid steel of casting billet. And because of a greater degree of supercooling in the mould, liquid steel solidify immediately to form a thin shell. a large number of crystal nucleus is formed, but grain growth is inhibited because of the temperature decreasing rapidly, A layer of thin and fine equiaxed grain in the shell, as shown in figure.3a1 and 3b1. With the increasing of casting time, the shell thicken gradually, due to the degree of supercooling is reduced during this process, grain growth increase relatively while nucleation slow down, developed dendrite grain is produced on the region of the wide cross section, as shown in **Fig.5-a2** and **b2**. However, heat large lose in the casting slab with casting time increase. On the one hand, the temperature will be below the liquidus temperature in the central area of casting slab, which led to more grain nucleus form. On the other hand, secondary grain endings are erosion by liquid steel of high temperature, fused grain endings become source of nucleation. And growth rate of grain nucleus are equal, so the equiaxed grains are produced at the central area of casting, as shown in **Fig.5b-a3** and **b3**.

2.4.1 Results and Analysis of Flow field

Fig.6 is the velocity distribution of the middle face of the mold wide surface. As shown in Fig.6, high velocity jet of high temperature molten steel is formed with a certain injection rate in the submerged nozzle. Velocity is constantly dissipation in the process of impact on the narrow surface of the mould, initial velocity of liquid steel is 1.35m·s^{-1} at the inlet of submerged nozzle, the velocity value is less than 0.4 m·s^{-1} when the molten steel arrive at the bottom of the mould. the stream is divided into two parts of high and low streams when the molten steel impact to narrow surface of the mould(the distance from the meniscus is 0.38m) because of changing in the direction of velocity. the upper recirculation region is formed because high stream is encumbered by the meniscus and then flow through sub-liquid level to wall surface of the submerged nozzle. this stream directly affects the fluctuation of the free surface, the melting and involvement of the mould powders, the growth of the solidified shell. At the same time, the lower recirculation region become a larger because of flowing though narrow surface of the mould(casting direction) to the center of the molten steel, and then flows from down up. It has a positive impact on the rise of the slag

inclusion and the inner bubbles. **Fig.6 (c)** shows the streamline distribution of molten steel in mould, considering the influence of the solidified shell, free-flowing space of lower recirculation region is reduced owing to limiting flow of molten steel. And according to Energy conservation principle, Energy is increased in the upper recirculation region. In addition, growth speed of the initial solidified shell is slow in the upper recirculation region, a thin shell is only formed, the inhibitory effect is not obvious to the fluid flow of the upper recirculation region. In short, considering effect of the solidified shell on the flow of molten steel, the space of flow has not noticeably altered at the upper recirculation region, but the vortex center of the lower recirculation region move from the edge to the center. Intensity of recirculation regions is related to nozzle angle, nozzle diameter, immersion depth and casting speed, etc. It forecast that the rational distribution of flow field could pass the optimization of structure parameters and technical parameters.
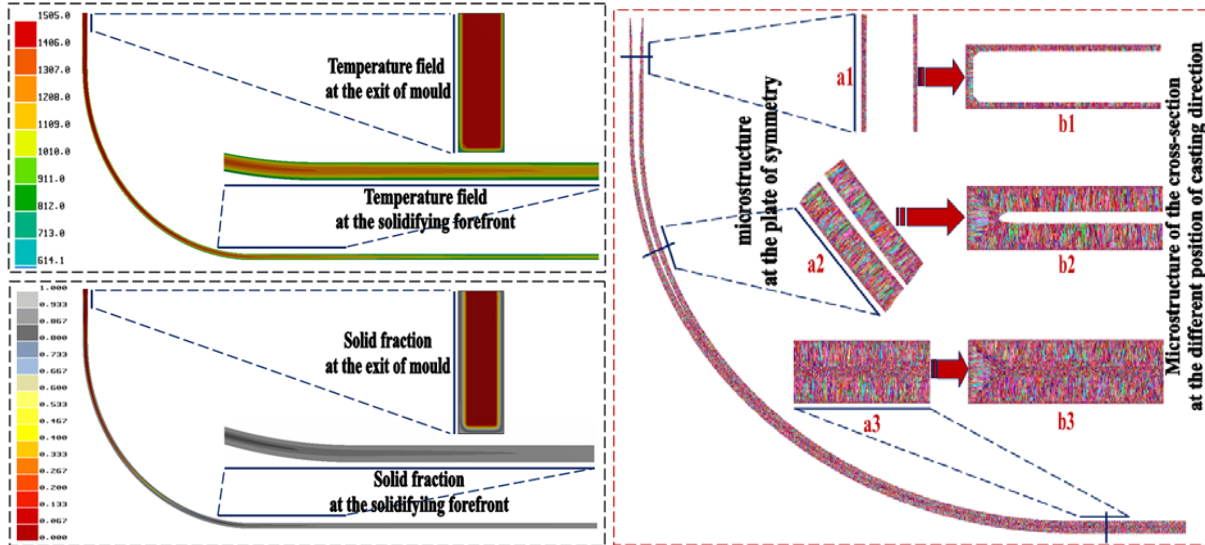

Fig.5 The temperature field, he solid fraction when the slab is reaching steady state and Schematic diagram of evolution of solidification microstructure of the slab cross and longitudinal section
(a) The temperature field and the solid fraction; (b) Schematic diagram of evolution of solidification microstructure
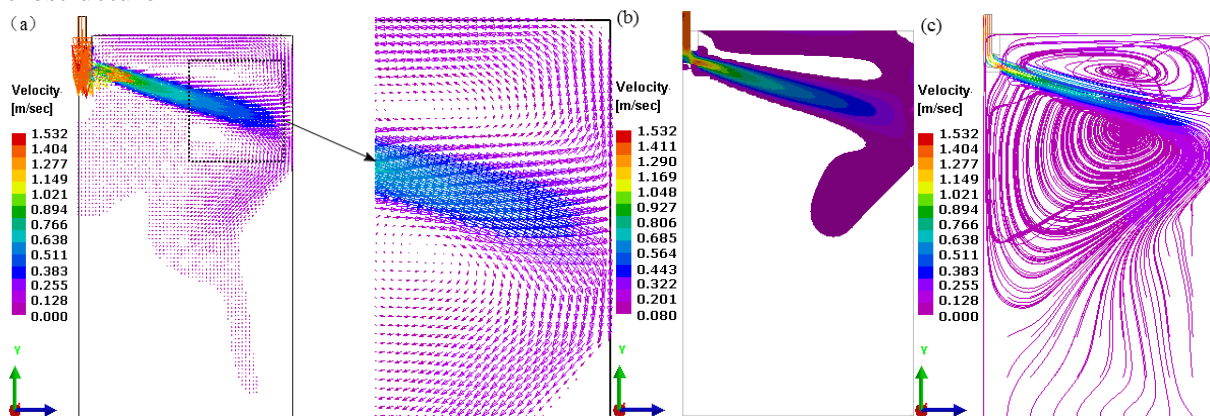

Fig.6 Velocity distribution of the middle face of the mold wide surface.(a)the contour of velocity vector,(b)the contour of velocity when V＞0.08 m·s-1,(c)the contour of streamline

2.4.2 Results and Analysis of Temperature field

Fig.7 shows temperature distributions of different cross sections solidified shells and fraction solid distribution. Owing to cooling of the mould, three kinds of Existence states are formed for high temperature liquid steel: liquid (crimson zone), solid (grey zone) and mushy zone (orange and yellow zone). according to the assumption, Only two dimensional heat transfers (lateral direction) is considered. temperature at the corners is lowest because high temperature liquid steel are affected by the cooling of wide face and narrow face at the same time. Therefore, the shell is thickest at the corners. But the narrow face is affected by high temperature owing to high temperature stream, the formation of temperature gradients can lead to the smallest shell at the center of narrow face, is only

10.4mm, as shown in Fig.8e. At the wide face, the solidified shell, is thicker than the narrow face in the same cross section, which is 18.9mm (above 0.8 solid fraction) at the center, and the shell thickness is 24.7mm when the solid fraction is greater than 0.667, as shown in Fig.7f.

In actual industrial production, solidification shrinkage is serious at the corners of the mould, the formation of air gap could lead to produce larger thermal resistance so that shell thickness at the off-corner of the mould is reduced, and then the corners cracks and leakage accidents are produced. Under the designed parameters conditions, on the cross section width to the thickness of solidified shell is more reasonable at the wide face of 0.8m distance from the meniscus, but the shell thickness is small at the narrow face, therefore, the cooling water appropriately increase to improve the thickness of narrow face. Temperature of the billet center is almost constant because the molten steel has a greater superheat. Central temperature of the wide face decrease smoothly, the temperature is 1014.6°C at the exit of mould. Highest temperature appeared at the Center of the narrow face, the distance 0.4m from the meniscus. because the impact point of the nozzle flows at a distance of 0.38 m from the meniscus.
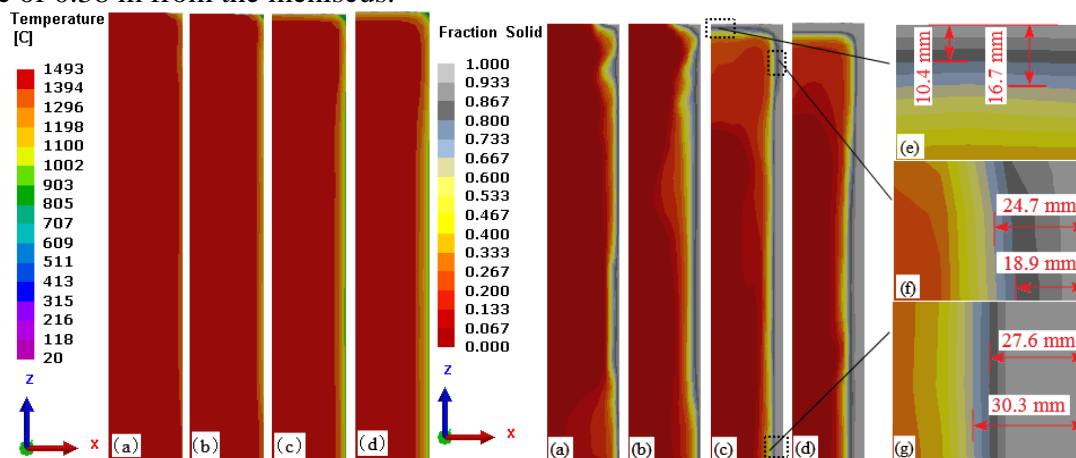

Fig.7 Temperature distributions of different cross sections solidified shells and fraction solid distribution. The distance from meniscus is (a)0.3m,(b)0.5m,(c)0.8 m,(d)1.5m; (e),(f),(g) Partial enlarged views of three positions in the (c)

3. Conclusion

Casting process of the 2400 mm×400 mm extra-thick Steel slab is analyzed by a three-dimensional steady-state physical model and moving boundary algorithm built on Pro-CAST software , the microstructure and sump depth are validated by theoretical and experimental results. Through analysis of the simulation results, several important information can be concluded as follows:

a)   Based on the conditions of 0.54m/min casting speed and 20°C superheat, a smaller special water flow is conductive to the equiaxed grains growth in the secondary cooling region.

b)   under the optimized parameters, such as casting speed, superheat degree and secondary cooling intensity. For the cross section at the exit of mould, the center thickness of narrow face is 16.7mm, thickness near the corner is 24.7 mm, the center thickness of wide surface is 30.3 mm.

The corresponding author: Yibo Li, Email: yibo.li@csu.edu.cn. The first author: Pinghu Chen, Email: chenpinghu1986@163.com

Reference

[1] Wen-hong LIU, Zhi XIE a, Zhen-ping JI, Biao WANG, Zhao-yi LAI, Guang-lin JIA. Dynamic Water Modeling and Application of Billet Continuous Casting[J]. JOURNAL OF IRON AND STEEL RESEARCH, INTERNATIONAL, 2008,15(2):14-17.

[2] Fengming Du, Xudong Wang, Man Yao, Xiaobing Zhang. Analysis of non-uniform thermal behavior in slab continuous casting mold based on the inverse finite-element model[J]. Journal of Materials Processing Technology, 2014, 214:2676-2683.

[3] Zhaofeng Wang, Man Yao, Xudong Wang, Xiaobing Zhang, Longsheng Yang, Hongzhou Lu, Xiong Wang. Inverse problem-coupled heat transfer model for steel continuous casting[J]. Journal of Materials Processing Technology, 2014, 214, 44-49.

[4] Hong Chen, Litao Su, Guangjun Wang, Shibin Wan, Lihui Zhang, Zhaoming Luo. Fuzzy estimation for heat flux distribution at the slab continuous casting mold surface[J].International Journal of Thermal Sciences, 2014, 83: 80-88.

[5] Johne Jesus Mol Peixoto, Weslei Viana Gabriel, Leticia Queiroz Ribeiro, Carlos Antônio da Silva, Itavahn Alves da Silva, Varadarajan Seshadri. Computational and physical simulation of fluid flow inside a beamblank continuous casting mold[J]. Journal of Materials Processing Technology, 2016, 233: 89-99.

[6] Huijun Feng, Lingen Chen, Zhihui Xie, Zemin Ding, Fengrui Sun. Generalized constructal optimization for solidification heat transfer process of slab continuous casting based on heat loss rate[J]. Energy, 2014, 66: 991-998.

[7] Jha AMaPK. EFFECT OF CASTING SPEED ON CONTINUOUS CASTING OF STEEL SLAB[J]. International Journal of Mechanical Enmineering and Robotics Research, 2014, 1(1): 13-21.

[8] R.Vertnik BS. Solution of a continuous casting of steel benchmark test by a meshless method[J]. Engineering Analysis with Boundary Elements, 2014, 45: 45-51.

[9] Jian Zhang, Deng-Fu Chen, Cheng-Qian Zhang, Shui-Gen Wang,Weng-Sing Hwang, Ming-Rong Han. Effects of an even secondary cooling mode on the temperature andstress fields of round billet continuous casting steel[J]. Journal of Materials Processing Technology, 2015, 222: 315-326.

[10]M. RYWOTYCKI, K. MIŁKOWSKA-PISZCZEK, L. TREBACZ. IDENTIFICATION OF THE BOUNDARY CONDITIONS IN THE CONTINUOUS CASTING OF STEEL," ARCHIVES OF METALLURGY AND MATERIALS, 2012, 57(1):385-393.

[11]QU Tian-peng, WANG Shui-gen, FENG Ke. Numerical simulation on solidification microstructure of Bloom During Continuously casting process[J]. Continuous Casting, 2013, 6: 7-11.

[12]Nan WANG, Jian-hong DONG, Wei-jun HUANG, Bo LI, Min CHEN. Growth Rate, Microstructure and Phase Composition of Oxide Scales for Three Typical Steels in Simulated Continuous Casting Process[J]. JOURNAL OF IRON AND STEEL RESEARCH, INTERNATIONAL, 2014, 21(12):1065-1072.

[13]J. Z enisek, E. Kozeschnik, J. Svoboda, and F.D. Fischer. Modelling the role of compositional fluctuations in nucleation kinetics[J]. Acta Materialia, 2015,91:365–376.

[14]Bastian Rheingans, EricJ.Mittemeijer. Modelling precipitation kinetics: Evaluation of the thermodynamics of nucleation and growth[J]. CALPHAD: Computer Coupling of Phase Diagrams and Thermochemistry, 2015, 50:49-58.

[15]Sen LUO, Miaoyong ZHU and Seppo LOUHENKILPI. Numerical Simulation of Solidification Structure of High Carbon Steel in Continuous Casting Using Cellular Automaton Method[J]. ISIJ International, 2012, 52 (5): 823–830.

[16]PANG Ruipeng, WANG Fuming , ZHANG Guoqing, LI Changrong. Study of solidification thermal parameters of 430 ferrite stainless steel based on 3D-CAFÉ method[J]. Acta Metallurgica Sinica, 2013, 49(10): 1234-1242.

[17]Jian Zhang D-FC, Cheng-Qian Zhang, Shui-Gen Wang,Weng-Sing Hwang. Dynamic spray cooling control model based on the tracking of velocity and superheat for the continuous casting

steel[J]. Journal of Materials Processing Technology, 2016, 229: 651-658.